

Effect of Thermomechanical Treatment on Microstructure and Mechanical Properties of ASTM A615/A615M Grade-60 Steel Reinforcement Bars

Syed Ali Afzal, Subhan Jogi*, Tufail Ahmed, Abdul Qadir, Vinod Kumar and Zubair Laghari

Department of Metallurgy and Materials Engineering,
Dawood University of Engineering and Technology, Karachi, Pakistan

(received June 20, 2022; revised April 7, 2023; accepted April 14, 2023)

Abstract. The purpose of this research is to manufacture steel rebars per the obligations declared in ASTM A615/615M Grade-60 *via* hot rolling of steel billets and thermomechanical treatment process installed at the manufacturing facility. Afterward, to understand the effect of processing parameters on the microstructure and mechanical properties of the finished product. The characterization of rebars include the chemical analysis of the final product. Moreover, the average yield strength, ultimate tensile strength, yield strength and ductility were examined. Furthermore, 180° bend testing, Charpy V-notch test, hardness, scanning electron microscopy (SEM) and optical microscopy were also explored. The results show the product perfectly endorses the demand of the standard and the values are within the specified range. But the material demonstrates menial impact energy and the characteristic features of the brittle fracture. Furthermore, hardness testing, optical microscopy and SEM corroborate the existence of dissimilar microstructures in the vicinity of core and case areas. The results shows the material satisfy the ASTM A615/615M grade-60 standard, but exhibit inferior energy absorption capabilities.

Keywords: hot rolling, thermomechanical treatment, reinforcement bars, tempered martensite, pearlite

Introduction

There is soaring interest among the reinforced concrete manufacturers to employ greater strength steel reinforcement bars (rebars) for lightweight yet indestructible gigantic structures (Cortsen *et al.*, 2014). This fascination is propelled essentially by the exceptional mechanical properties of steel bars in slabs, beams, footings and columns, especially in the construction of buildings capable to withstand the deadliest earthquakes (Wang *et al.*, 2022). The foremost responsibility of reinforced steel is to strengthen the concrete matrix by letting it bend to some degree, and avert failure amid the tensile loading situations (Huq, 2018). Deformed steel bars are used as reinforcement in concrete to enhance ductility and cease the crack propagation within the structure. In the contemporary world, structural steel is utilized in the construction of colossal residential and commercial buildings, offshore platforms, warehouses, bridges and others (Seliem *et al.*, 2009). Besides, the mechanical properties of steel can be altered by numerous methods. For instance, modifying the chemical make-up, inducing plasticity and strength via cold-working, tuning the hard and soft phases inside the microstructure, quenching

and tempering, and amending the metastable fractions (Gao *et al.*, 2021; Zhang *et al.*, 2021; Singh *et al.*, 2020). Additionally, the yield strength of steel rebars is a crucial factor for both the manufacturer and the end-user. Hot rolling imparts alteration in the microstructure and boosts functional properties of rebar (Roberts, 1983). Reinforcement bars manufactured by way of thermomechanical treatment (TMT) manifest a superior heat treatment process in which rebars coming out of the finishing mill at elevated temperature are quickly quenched across water spraying nozzles. The phase transformation occurs by the introduction of a large number of defects during rolling and TMT, which act as nucleation sites and assist the process of diffusion (Duckworth, 1966). TMT offers rigorous cooling of surface which results in the rebars containing surface of high hardness with a core of excellent toughness. After that, the rebars are allowed to cool in the air until room temperature is reached. In the course of slow cooling in the air, the energy in the form of heat discharged from the core changes the microstructure at the surface and at the same time, the core transforms into a combination of ferrite and pearlite (Saastamoinen *et al.*, 2017). The final microstructure after the TMT process is a composite of soft ferrite-pearlite in the core

*Author for correspondence;

E-mail: subhan.jogi@duet.edu.pk

along with hard tempered martensite at the surface (Ahmed *et al.*, 2021). The above mentioned coalition of microstructures contributes an ideal merger of superior strength, ductility, toughness and other necessary properties (Yadav and Ale, 2021; Schastlivtsev *et al.*, 2015). Fabrication of engineering structural materials by low-alloy steels is intended to bestow austenite microstructure, followed by quenching and tempering process or meticulous cooling resulting in a ferrite-pearlite microstructure. This study is conducted on ASTM A615/A615M grade-60 reinforcement steel bar (ASTM-A615/A615M, 2020) manufactured by rolling mill and TMT process at Faizan Steel. Faizan Steel is Pakistan's fastest growing producer of deformed steel bars, with a state-of-the-art automatic rolling machine, generating over 600 tonnes of high quality deformed steel bars daily. A comprehensive study was accomplished to establish the consequences of specified TMT parameters adopted by the manufacturing facility such as bar diameter, mill speed, number of passes and nozzle pressure on the overall mechanical properties as well as the disparity of the microstructure between the core and the case of grade-60 reinforcement bar. Ample knowledge of the collective outcome of rolling and TMT on the properties of steel reinforcement bars will benefit in determining the optimum process conditions to attain outstanding in-service properties.

Table 1. Operating parameters of rolling mill and TMT box during the production of $\varnothing 25$ mm rebar

Nominal diameter (θ) of Rebar	25 mm
Number of pass(es) in Roughing mill	1
Roughing mill Speed	2.8 m/s
Number of pass(es) in Intermediate mill	4
Intermediate mill speed	3.0 m/s
Number of pass(es) in Finishing mill	2
Finishing mill Speed	3.35 m/s
Number of nozzles in TMT box	4
Nozzle pressure	7.5-9 bars
Nozzle diameter	42 mm

Material and Methods

The reinforcement bars of specification ASTM A615/615M grade-60 (ASTM-A615/A615M, 2020) having a nominal diameter of 25 mm are selected for the evaluation. The raw material for the rebars was steel billets of dimensions 100 mm \times 100 mm. The billets were heated in the re-heating furnace to about 1100 °C to 1150 °C and then transferred to the rolling mill which is divided into three categories *i.e.* Roughing mill, Intermediate mill and Finishing mill. After the Finishing mill, the rebar was sent to 22 meters long TMT box for controlled water quenching. The temperature of the rebar was maintained around 750 °C before introducing into the TMT box. The number of passes during rolling and other operating parameters during the TMT process are summarized in Table 1.

The chemical composition of the rebar was analyzed by spark Optical Emission Spectrometer (OES) in accordance with ASTM E415 (ASTM-E415, 2021). The average chemical composition of the rebar is presented in Table 2. All the elements conform to the obligations of ASTM A615/A615M grade-60 (ASTM-A615/A615M, 2020), especially phosphorous, which must be = 0.06%. Three measurements were taken and their average was considered as the final chemical composition. All the mechanical tests were carried out according to ASTM A370 (ASTM-A370, 2021). The tension tests and Bend tests were performed on three full sections rolled rebar samples using Universal Tensile Testing Machine (UTM) to evaluate the yield strength (YS), ultimate tensile strength (UTS) and ductility (% elongation). However, to interpret % elongation, gage length was taken as 200 mm. Moreover, the 180° Bend test was also executed on three samples using a round bending pin of diameter 125 mm. Rockwell hardness testing (HRB) was used to measure hardness in the vicinity of the surface (case) and core. The hardness values were taken at the cross section of the rebar in the core area and the same is repeated for the area in the vicinity of the surface to assess the hardness contrast.

Table 2. Chemical composition (wt %) of the rebar under study (average of three measurements)

C	Si	Mn	P	S	Cu	Al	Cr	Mo	Ni	V
0.257	0.296	1.017	0.029	0.033	0.245	<0.001	0.195	<0.001	0.054	<0.001
Fe	Nb	Co	W	Sn	Pb	B	As	Zr	Zn	Ti
97.8	<0.001	0.003	<0.001	<0.005	<0.001	0.0016	0.002	<0.001	0.012	<0.001

The Charpy Impact Test was executed at room temperature. Specimen of dimensions 55 mm × 10 mm × 10 mm with a V-shaped notch of 45° at the center and 2 mm depth was machined along the rolling axis of the rebar. The equipment used for the impact test was “JB-500B Pendulum Impact Testing Machine”. The distance between the pendulum center and impact point was 800 mm and the impact velocity was 5.4 m/s. The scanning electron microscopy (SEM) and optical microscopy (OM) was accomplished on the same transverse sections of rebar as the hardness. The specimen was cold mounted, mechanically grinded and polished using alumina paste for the SEM analysis. Furthermore, the specimen was chemically etched with 2% Nital solution for 5 sec for metallographic examination in consonance with ASTM E883 (ASTM-E883-11, 2017). The microstructure of the core and case region was examined via both microscopy techniques.

Results and Discussion

The confirmation of tensile properties ASTM standard E8 specimen placed in middle of the upper and lower cross head of (Zwick Roell-250KN) Universal Tensile Machine. UTM works in principle when upper cross

head is transportable whereas lower cross head stationary (Sharven, 2022). The equipment has controlled by electronic load cell by setting its parameters for the study yield and tensile strength of the E8 standard samples (Hanson 2022). For destructive testing strain rate adjusted of 2.8×10^{-4} /sec, specimen stretched out in length and reduced in cross-section. The results of the Tension Test of three rebar samples and their minimum standard value are shown in Table 3 and graphically represented in Fig. 1.

The YS and UTS of all samples are above 420 MPa and 550 MPa respectively. In addition, the mean of UTS/YS ratio comes at 1.37. The % elongation also exceeds the nominal standard threshold. All of the parameters are way beyond the baseline values and conform to the ASTM A615/615M grade-60 standard.

The Bend Test also reveals the ability of the rebar to form a 180° bend as shown in Fig. 2. This uncovers the excellent ductility of the material and also supports the average % elongation of 18.4% as shown in Table 3.

The hardness readings were undertaken inside the regions highlighted in Fig. 3. The average hardness of the core is 86 HRB, whereas the average hardness of

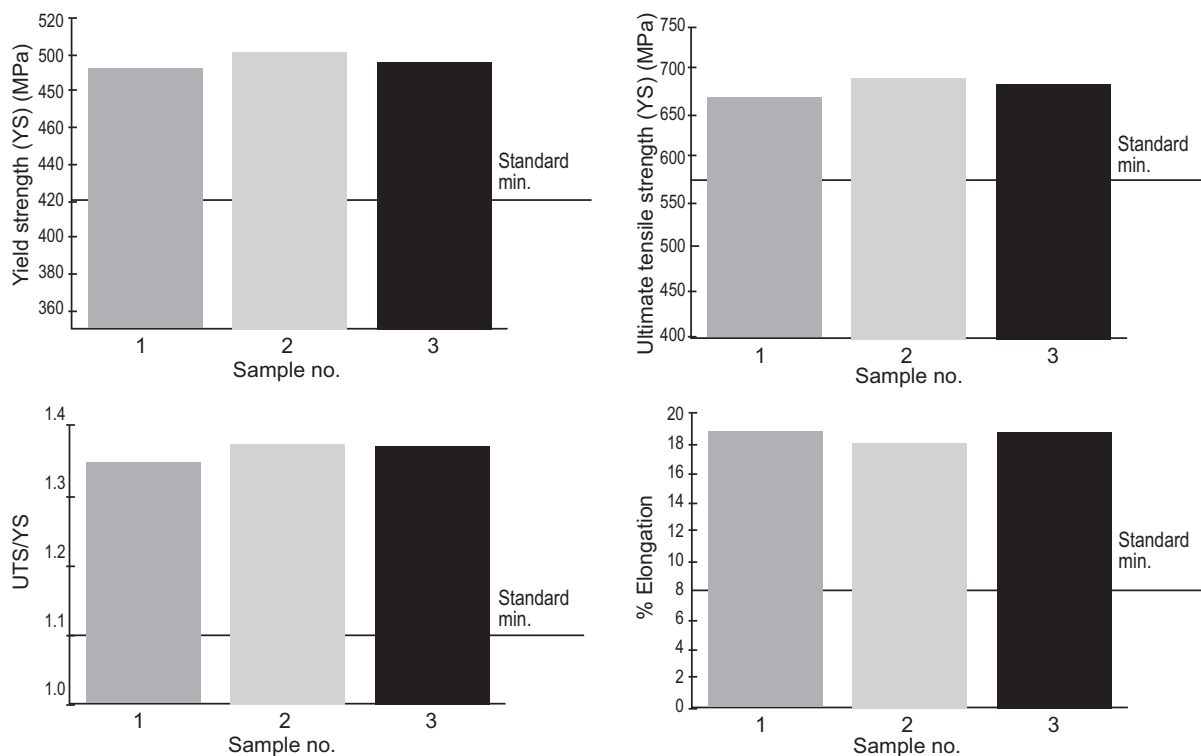


Fig. 1. Graphical representation of Tension test results for 3 samples.

Table 3. Tension test results of rebar samples along with standard values

Sample nos.	Yield strength (YS) (MPa)	Ultimate tensile strength (UTS) (MPa)	Ratio of UTS to YS	Elongation (%)
1	492	664	1.35	18.7
2	501	688	1.37	17.9
3	495	682	1.37	18.6
Average	496	678	1.37	18.4
Standard value (min)	420	550	1.1	8

the case comes at 99 HRB. This disparity among the hardness values is attributed to the different microstructures in the core and case regions (Ahmad and Sajal, 2020; Kabir and Islam, 2014) and will be discussed in detail in the microstructure section.

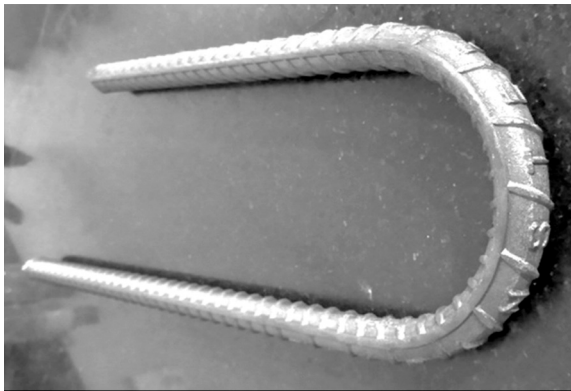


Fig. 2. Rebar after bend test.

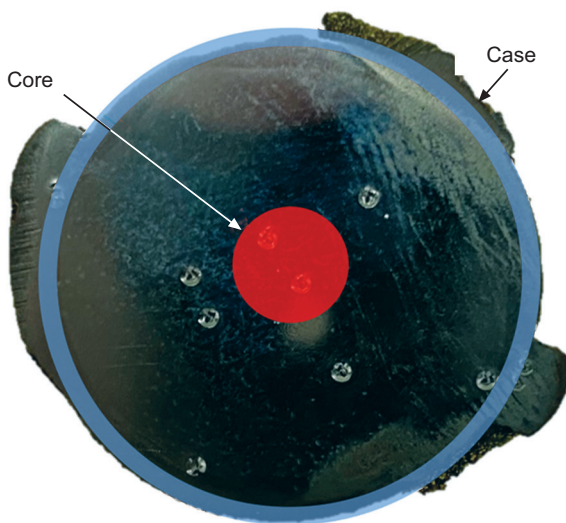


Fig. 3. Hardness and microstructure evaluation locations.

In Fig. 4(a) the outcome of the Charpy V-notch test demonstrates that the specimen failed in a brittle manner when subjected to impact loading. The impact energy was found to be 25 J. The fractured surface of the specimen displays characteristics of brittle fracture as shown in Fig. 4. Moreover, the fracture surface in Fig. 4(b) exhibits a shiny surface without any appreciable plastic deformation. The grain like appearance also indicates that the mode of fracture is transgranular as a result of changes in orientation of the cleavage planes from grain to grain (Inoue *et al.*, 2021; Callister and Rethwisch, 2007). Accordingly, to validate the brittle behaviour, the hardness measurements were taken on the broken specimen at locations H1, H2 and H3. The average hardness was found to be 92 HRB on the fractured sample which is relatively higher than the hardness of core. The higher hardness measurement is the evidence of a contrasting microstructure as compared to the soft core, which could be the driving

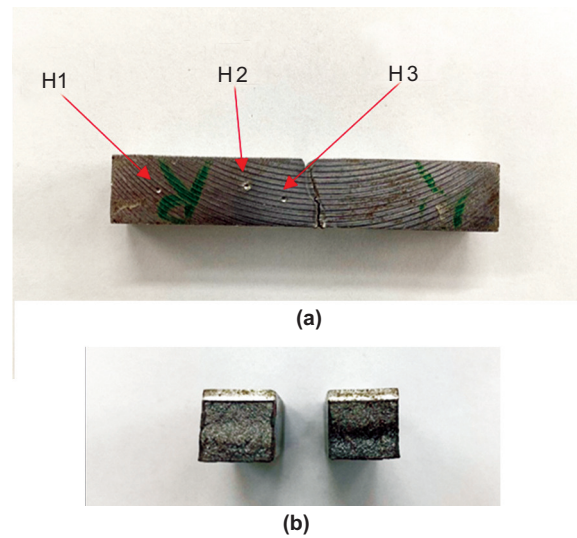


Fig. 4. Charpy V-notch specimen (a) showing negligible plastic deformation after impact test, (b) fractured surface.

factor for the brittle nature of fracture under the influence of sudden load. Hence, it could be concluded that the rebar's performance will be inferior for the applications where impact loading is dominant.

The microstructural features of the core and case are displayed in Fig. 5 at a magnification of 100x. The optical micrograph at the core shown in Fig. 5(a) consists of a combination of equiaxed grains of polygonal ferrite (white areas) and pearlite (dark areas) (Ray *et al.*, 1997). Moreover, the hardness value also authenticates the microstructure findings at the core (Ahmad and Sajal, 2020; Avner, 1974). On the contrary, due to the drastic cooling rate at the surface inside the TMT box, the case presents a very fine microstructure similar to tempered martensite (Kabir and Islam, 2014) as revealed in Fig. 5(b) but it is not possible to resolve tempered martensite at 100x magnification. Despite the agreement between case micro-structure and the hardness of

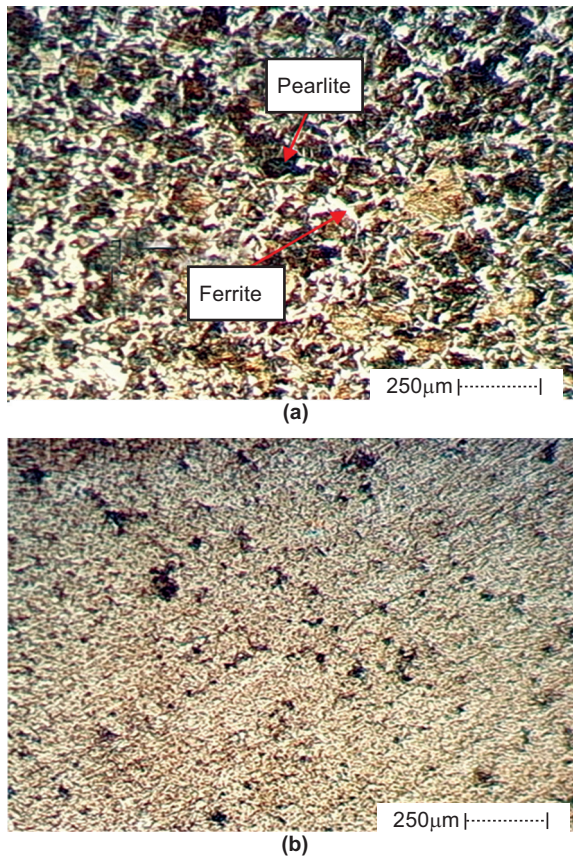


Fig. 5. Optical micrographs of transverse section of $\phi 25$ mm rebar at 100x showing (a) core and (b) case.

tempered martensite, SEM is also employed on the specimen to interpret and confirm the micro-structures at higher magnification.

The SEM images of the core and case areas at a magnification of 3000x are presented in Fig. 6. In the core region displayed in Fig. 6(a), a combination of proeutectoid ferrite and pearlite is clearly visible. The proeutectoid ferrite transpires due to the presence of carbon significantly less than the eutectoid point and can be confirmed by the results of spectroscopy. Additionally, the lamellar structure of pearlite consists of ferrite background and thin plates of cementite (Fe_3C) (Barani *et al.*, 2007; Metallography and Microstructures, 2004; Avner, 1974). Likewise, the Widmanstatten ferrite also appears on the microstructure, which is typical of the rebars manufactured by thermomechanical treatment

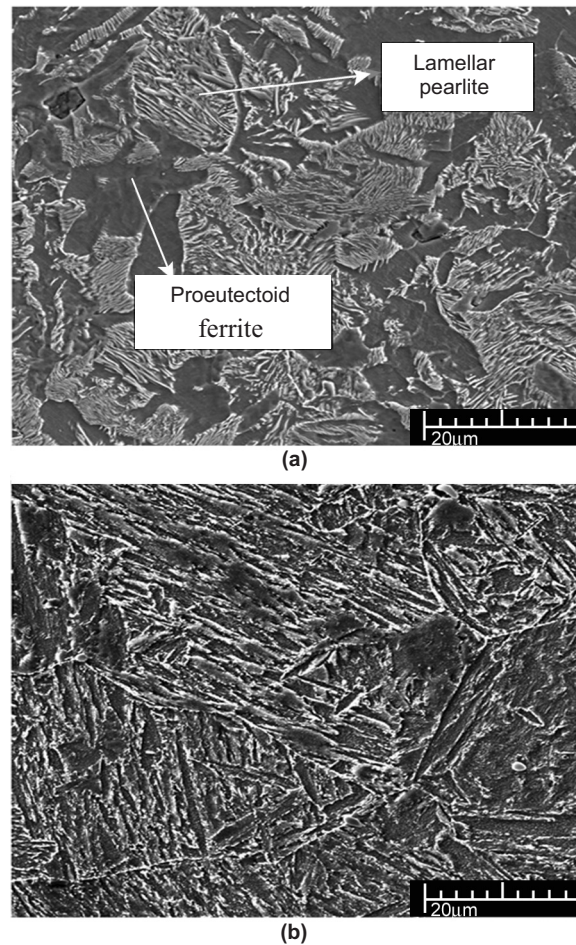


Fig. 6. SEM micrographs of transverse section of $\phi 25$ mm rebar at 3000x showing (a) core and (b) case.

and aids in the improvement of tensile strength (Katiyar *et al.*, 2019; Barani *et al.*, 2007). However, the higher amount of Widmanstätten ferrite could have resulted in the improved impact behaviour (Mintz, 2020). Alternatively, the microstructure at the case is comprised of tempered martensite and bainite (Schastlivtsev *et al.*, 2015; Metallography and Microstructures, 2004) as displayed in Fig. 6(b). The reason for this distinctive microstructure is that the fast-quenching process inside the TMT box engenders the formation of brittle body-centered tetragonal (BCT) martensite at the surface. However, the auto-tempering process due to the heat flowing from the core towards the case transforms the martensite to a blend of hexagonal close-packed transition carbide, also known as epsilon carbide and low-carbon martensite. Similarly, any additional retained austenite is transformed to bainite (Avner, 1974).

Conclusion

To recapitulate, the steel reinforcement bars of $\phi 25$ mm are manufactured by re-rolling and thermomechanical treatment (TMT) process in accordance with the specified process parameters. The chemical composition conforms to the manufacturing standard, especially phosphorous, which is found to be 0.029%. The average yield strength (YS), ultimate tensile strength (UTS) and % elongation is 496 MPa, 678 MPa and 18.4% respectively. UTS/YS ratio and 180° Bend Test also uphold the requirements mentioned in ASTM A-615/615M Grade-60. Nevertheless, the Charpy V-notch Impact Test revealed the brittle nature of the sample under the influence of impact loading and the impact toughness is merely 25 J. In addition, hardness testing, optical microscopy, and SEM validate the presence of contrasting micro-structures near the core and case regions. The microstructure at the core is a merger of ferrite and pearlite with a hardness of 86 HRB. Whereas, the microstructure at the case is a combination of tempered martensite and bainite, exhibiting the hardness of 99 HRB.

Acknowledgement

We would like to present our heartfelt gratitude to Engr. Muhammad Hadi Hanif and Engr. Saqib Aslam at Faizan Steel, Karachi, Pakistan, for their cooperation throughout the project. We would also like to thank The Department of Metallurgical Engineering, NED University of Engineering and Technology, Karachi, Pakistan for their support to carry out various characterization techniques.

Conflict of Interest. The authors declare that they have no conflict of interest.

References

- Ahmed, E.S., Ibrahim, M., Galal, S.A., Elnekhaily, Allam, T. 2021. Microstructure and mechanical properties of V-alloyed rebars subjected to Tempcore process. *Metals*, **11**: 246.
- Ahmad, S., Sajal, W.R. 2020. An experimental investigation of relationship between surface hardness and strength of locally produced TMT 500W bar in Bangladesh. *Journal of Engineering Science*, **11**: 113-122.
- ASTM-A370. 2021. *Standard Test Methods and Definitions for Mechanical Testing of Steel Products*: ASTM International, West Conshohocken, Pennsylvania, USA.
- ASTM-E415. 2021. *Standard Test Method for Analysis of Carbon and Low-Alloy Steel by Spark Atomic Emission Spectrometry*: ASTM International, West Conshohocken, Pennsylvania, USA.
- ASTM-A615/A615M. 2020. *Standard Specification for Deformed and Plain Carbon-Steel Bars for Concrete Reinforcement*: ASTM International, West Conshohocken, Pennsylvania, USA.
- ASTM-E883-11. 2017. *Standard Guide for Reflected-Light Photomicrography*: ASTM International, West Conshohocken, Pennsylvania, USA.
- Avner, S.H. 1974. *Introduction to Physical Metallurgy*, 2nd edition, pp. 353, McGraw-hill, New York, USA.
- Barani, A.A., Li, F., Romano, P., Ponge, D., Raabe, D. 2007. Design of high-strength steels by microalloying and thermo-mechanical treatment. *Materials Science and Engineering: A*, **463**: 138-146.
- Brett, A., Miller, Roch, J. Shipley, Ronald, J. Parrington, Daniel, P., Dennis, B. 2021. *Failure Analysis and Prevention*. vol. **11**: pp. 856, ASM International, Los Angeles, California, USA.
- Callister, W.D., Rethwisch, D.G. 2007. *Materials Science and Engineering: an Introduction*, 4th edition, pp. 975, John Wiley & Sons, New York, USA.
- Cortsen, J., Rytz, J.A., Ellekilde, L.-P., Sølvason, D., Petersen, H.G. 2014. Automated fabrication of double curved reinforcement structures for unique concrete buildings. *Robotics and Autonomous Systems*, **62**: 1387-1397.
- Duckworth, W. 1966. Thermomechanical treatment of metals. *Journal of the Minerals, Metals and Material Society*, **18**: 915-922.

- Gao, B., Hu, R., Pan, Z., Chen, X., Liu, Y., Xiao, L., Cao, Y., Li, Y., Lai, Q., Zhou, H. 2021. Strengthening and ductilization of laminate dual-phase steels with high martensite content. *Journal of Materials Science AND Technology*, **65**: 29-37.
- Hanson, S.A. 2022. The tempering response of CPM® 3v tool steel investigated through tensile testing and micro-structural observations. *Crystals*, **12**: 1670.
- Huq, M.S. 2018. *High-Strength Steel Bars in Earthquake-Resistant T-Shaped Concrete Walls*. University of Kansas, American Concrete Institute, KU Scholarworks.
- Inoue, T., Qiu, H., Ueji, R., Kimura, Y. 2021. Ductile-to-brittle transition and brittle fracture stress of ultrafine-grained low-carbon steel. *Materials*, **14**: 1634.
- Kabir, I., Islam, M. 2014. Hardened case properties and tensile behaviours of TMT steel bars. *American Journal of Mechanical Engineering*, **2**: 8-14.
- Katiyar, P.K., Behera, P.K., Misra, S., Mondal, K. 2019. Comparative corrosion behaviour of five different micro-structures of rebar steels in simulated concrete pore solution with and without chloride addition. *Journal of Materials Engineering and Performance*, **28**: 6275-6286.
- Mintz, B., Qaban, A., Naher, S. 2020. Further insights on compositional control and heat treatment for improving the impact behaviour of hot-rolled steels containing Nb and Al. *Materials and Design*, **190**: 108601.
- Ray, A., Mukerjee, D., Sen, S., Bhattacharya, A., Dhua, S., Prasad, M., Sahu, A. 1997. Microstructure and properties of thermomechanically strengthened reinforcement bars: a comparative assessment of plain-carbon and low-alloy steel grades. *Journal of Materials Engineering and Performance*, **6**: 335-343.
- Roberts, W.L. 1983. *Hot Rolling of Steel*, 2nd edition, pp. 1024, CRC Press, Boca Raton, Florida, USA.
- Saastamoinen, A., Kaijalainen, A., Porter, D., Suikkanen, P. 2017. The effect of thermomechanical treatment and tempering on the subsurface microstructure and bendability of direct-quenched low-carbon strip steel. *Materials Characterization*, **134**: 172-181.
- Schastlivtsev, V., Tabatchikova, T., Yakovleva, I., Reina, S.Y.D. g., Golosienko, S., Pazilova, U., Khlusova, E. 2015. Effect of thermomechanical treatment on the resistance of low-carbon low-alloy steel to brittle fracture. *The Physics of Metals and Metallography*, **116**: 189-199.
- Seliem, H.M., Hosny, A., Rizkalla, S., Zia, P., Briggs, M., Miller, S., Darvin, D., Browning, J., Gregory, M., Hoyt, K., Donnelly, K., James, O. 2009. *Bond Characteristics of ASTM A1035 Steel Reinforcing Bars*. American Concrete Institute Structural Journal, **106**: 530-539.
- Singh, N., Casillas, G., Wexler, D., Killmore, C., Pereloma, E. 2020. Application of advanced experimental techniques to elucidate the strengthening mechanisms operating in microalloyed ferritic steels with interphase precipitation. *Acta Materialia*, **201**: 386-402.
- Vander, V.G.F. 2004. *Metallography and Microstructures*. ASM International (9th edition), Los Angeles, California, USA. ISBN: 978-0-87170-706-2
- Wang, D., Wu, W., Fang, S., Kang, Y., Wang, X., Hu, W., Yu, H., Zhang, H., Liu, X., Luo, Y. 2022. Observation of polarity-switchable photoconductivity in III-nitride/MoSx core-shell nanowires. *Light: Science and Applications*, **11**: 1-13.
- Yadav, U., Ale, B.B. 2021. Study on mechanical properties of TMT bars manufactured in Nepal. *Journal of Advanced College of Engineering and Management*, **6**: 245-257.
- Zhang, H., Wang, W.-X., Chang, F., Li, C.-L., Shu, S.-L., Wang, Z., Han, Z., Zou, Q., Qiu, F., Jiang, Q. 2021. Microstructure manipulation and strengthening mechanisms of 40Cr steel via trace TiC nanoparticles. *Materials Science and Engineering: A*, **822**: 141693.